ISPRS Journal of Photogrammetry and Remote Sensing 128 (2017) 98–110

Contents lists available at ScienceDirect

ISPRS Journal of Photogrammetry and Remote Sensing

journal homepage: www.elsevier.com/locate/isprsjprs

Remote sensing estimation of colored dissolved organic matter (CDOM) in optically shallow waters

Jiwei Li [a], Qian Yu [a,*], Yong Q. Tian [b,c], Brian L. Becker [b,c]

[a] Department of Geosciences, University of Massachusetts, Amherst, United States
[b] Institute for Great Lakes Research, Central Michigan University, United States
[c] Department of Geography, Central Michigan University, United States

ARTICLE INFO

Article history:
Received 12 October 2016
Accepted 27 March 2017

Keywords:
CDOM
Carbon cycle
Optically shallow waters
Land-water interface
SBOP
Bottom effect index
Adaptive estimation approach

ABSTRACT

It is not well understood how bottom reflectance of optically shallow waters affects the algorithm performance of colored dissolved organic matters (CDOM) retrieval. This study proposes a new algorithm that considers bottom reflectance in estimating CDOM absorption from optically shallow inland or coastal waters. The field sampling was conducted during four research cruises within the Saginaw River, Kawkawlin River and Saginaw Bay of Lake Huron. A stratified field sampling campaign collected water samples, determined the depth at each sampling location and measured optical properties. The sampled CDOM absorption at 440 nm broadly ranged from 0.12 to 8.46 m^{-1}. Field sample analysis revealed that bottom reflectance does significantly change water apparent optical properties. We developed a CDOM retrieval algorithm (Shallow water Bio-Optical Properties algorithm, SBOP) that effectively reduces uncertainty by considering bottom reflectance in shallow waters. By incorporating the bottom contribution in upwelling radiances, the SBOP algorithm was able to explain 74% of the variance of CDOM values (RMSE = 0.22 and R^2 = 0.74). The bottom effect index (BEI) was introduced to efficiently separate optically shallow and optically deep waters. Based on the BEI, an adaptive approach was proposed that references the amount of bottom effect in order to identify the most suitable algorithm (optically shallow water algorithm [SBOP] or optically deep water algorithm [QAA-CDOM]) to improve CDOM estimation (RMSE = 0.22 and R^2 = 0.81). Our results potentially help to advance the capability of remote sensing in monitoring carbon pools at the land-water interface.

1. Introduction

Inland waters (streams, rivers and lakes) are responsible for transporting and transforming large amounts of carbon from terrestrial ecosystems to aquatic environments (Tranvik, 2014). Each year, inland waters emit about 1 gigaton of carbon as CO_2 to the atmosphere and transfer an equivalent amount of carbon to ocean waters (Battin et al., 2009). This flux is larger than originally estimated and more than half of it results from the movement of dissolved organic carbon (DOC) from terrestrial environments (Stedmon et al., 2000). Accordingly, riverine systems (streams and rivers) govern much of the DOC export from terrestrial to aquatic environments (IPCC, 2007) and dictate the spatial and temporal variability of freshwater DOC in drainage watersheds. Shallow coastal and estuarine areas are the primary interface regions for carbon exchange from terrestrial to aquatic ecosystems. The variations of terrestrial carbon exports in these regions are heavily associated with anthropogenic activities (Palmer et al., 2015). Therefore, increased attention is being devoted to carbon monitoring of optically shallow waters. Several studies have demonstrated that remote sensing technologies show great promise for monitoring freshwater DOC dynamics through bio-optical properties (Brezonik et al., 2015; Kutser et al., 2015; Olmanson et al., 2016; Zhu et al., 2015).

Colored dissolved organic matter (CDOM) is defined as the photoactive fraction of dissolved organic matters in water (Brando and Dekker, 2003). Light absorption by CDOM tends to be strongest at short wavelengths (ultraviolet to blue) while diminishing to near zero in the red wavelength region of the electromagnetic spectrum (Markager and Vincent, 2000). So CDOM level is often represented by a CDOM absorption coefficient within the highly absorbed short wavelengths, and 440 nm is frequently used by the remote sensing community (Brando and Dekker, 2003; Matsuoka et al., 2013;

* Corresponding author.
E-mail address: qyu@geo.umass.edu (Q. Yu).

http://dx.doi.org/10.1016/j.isprsjprs.2017.03.015
0924-2716/

Menon et al., 2011; Watanabe et al., 2016). Many previous studies have confirmed that CDOM levels are highly correlated to DOC concentrations in coastal & inland waters influenced by river discharge, regulated by terrestrial sources and seasonal effect (Del Castillo et al., 1999; Del Vecchio and Blough, 2004; Ferrari et al., 1996; Hestir et al., 2015; Kowalczuk et al., 2003). Therefore, CDOM is often used as a proxy to trace the spatial distribution of DOC so as to help quantify the transport of terrigenous organic carbon (Mannino et al., 2008). Thus, the quantitative estimation of CDOM absorption via remote sensing aids in the better understanding of carbon cycling at the land-water interface.

Most research efforts on the remote sensing of water biogeochemistry (CDOM, Chl-a and non-algal particles) have focused on the estimation of water bio-optical properties in open oceans (Lee, 2006; Mobley, 1999; Siegel et al., 2002). Generally, many of these remote sensing algorithms empirically utilize band ratios calibrated from regional datasets to retrieve water properties (Kutser et al., 2005; Matthews, 2011). However, they are often site-specific and need intensive calibration when applied to a new environment. Semi-analytical algorithms made a significant improvement to location independence by extracting water biochemical properties based on bio-optical radiative transfer models. Representative algorithms include multi-band quasi-analytical algorithm (QAA) (Lee et al., 2002), Carder-MODIS (Carder et al., 2004), Garver-Siegel-Maritorena (GSM) (Maritorena et al., 2010, 2002), and Linear Matrix (LM) model (Hoge and Lyon, 1996; Yang et al., 2011). Unfortunately, these algorithms cannot separate CDOM absorption from $a_{dg}(440)$, the combined absorption of CDOM and non-algal particles (NAP), due mainly to their similar absorption spectra. Recently, several studies endeavored to extend mainstream ocean color algorithms to derive CDOM absorption for coastal and open ocean waters (Budhiman et al., 2012; Cui et al., 2014; Matsuoka et al., 2013; Shanmugam, 2011; Zhu and Yu, 2013). However, when these relatively mature semi-analytical ocean color algorithms are directly applied to inland waters, the uncertainty of the resulting CDOM estimation is prohibitively high (Zhu et al., 2013b).

In general, there are two major challenges with the current semi-analytical algorithms used for CDOM retrieval of inland waters. First, the bottom effect of shallow freshwater introduces significant uncertainty on CDOM estimation. Ocean color algorithms are developed for optically deep waters, which assume the upwelling water leaving radiance is only the result of water column constituents and ignore bottom reflectance (Stedmon et al., 2000). This assumption is not valid for optically shallow inland and coastal waters, and therefore greatly limits the usage of these algorithms for inland waters (Aitkenhead-Peterson et al., 2003). Specifically, none of the aforementioned algorithms consider the contribution of bottom reflectance and therefore they are not capable of accounting for the high uncertainty introduced by bottom effects in optically shallow waters. Second, semi-analytical algorithms often incorporate empirical parameters into bio-optical models (water radiative transfer models). Such parameters are largely calibrated via ocean and offshore observations. Inland fresh waters are often much richer in water-borne constituents, (i.e., a higher concentration of CDOM, Chl-a and/or suspended sediment), so these algorithms are often not optimal for handling in-land water environments (Zhu and Yu, 2013; Zhu et al., 2013b). Except for a few cases, the majority of published research on CDOM retrieval in optically shallow lake waters adopt empirical methods (Campbell et al., 2011; Kutser et al., 2005, 2015; Odermatt et al., 2012; Olmanson et al., 2016).

Bottom effects have been considered in some aquatic remote sensing studies, including estimating water optical depth (Brando et al., 2009; Majozi et al., 2014; Maritorena et al., 1994; Zhao et al., 2013), retrieval of the diffuse attenuation coefficient (Barnes et al., 2014, 2013; Dekker et al., 2011; Giardino et al., 2015; Volpe et al., 2011), and monitoring bottom sediments properties (Klonowski et al., 2007). All of these approaches include the contribution of bottom sediment reflectance to the total upwelling radiance, which inspired us to develop a CDOM retrieval algorithm for optically shallow waters that also incorporates bottom reflectance.

First, this paper examines *in situ* spectral data and demonstrates the spectral variation in response to water depths. Second, we developed the shallow water bio-optical properties (SBOP) algorithm which incorporates the bottom contribution into a CDOM retrieval algorithm. Third, we investigated the effectiveness of a proposed bottom effect index (BEI) to quickly separate optically shallow and optically deep waters. Finally, an adaptive approach based on our BEI was presented to identify the most suitable algorithm according to varied levels of bottom effect (optically shallow or deep water algorithms) in an effort to reduce overall uncertainty. This study aims to improve the capability of remote sensing to monitor carbon transportation from terrestrial to aquatic ecosystems across broad spatial and temporal scenarios.

2. Method

2.1. Study site

Saginaw Bay in Lake Huron was selected for sampling CDOM levels concurrently with *in situ* remote sensing measurements across a broad range of CDOM levels. The sampling locations encompassed the Saginaw River, Kawkawlin River and inner Saginaw Bay (Fig. 1). The bathymetry ranged from 0.25 to 4 m with a median value of 1.6 m. Generally, the bottom is dominated by sand with intermittent patches of benthic algae (Cladophora) and other aquatic plants. Compared to that of pure sand, the sediments of the lake bottom are relatively dark due to this mixture of the sand and benthic plants. The two rivers mentioned above are of vastly different size and composition and their drainage basins are covered by different dominant vegetation. The Saginaw River is 36 km long with a watershed area of 22,260 km^2. The river has a mean annual discharge of 130 m^3/s (2010–2016). The dominant landcover type is agriculture, which accounts for approximately 52% of the watershed. The Kawkawlin River flows into the Saginaw Bay approximately 1 km north of the Saginaw River mouth. Its length (28 km), discharge and drainage area (647 km^2) are at a significant lower magnitude than those of the Saginaw River. The Kawkawlin River watershed is dominated by deciduous forest (40.2%) with a relatively high percentage of wetland (7.9%).

2.2. Field and laboratory measurements

A total of four cruises were carried out from 2012 to 2015. The cruises covered both spring and autumn seasons: May 7, 2015, May 7, 2013, May 10, 2012 and October 18, 2012. Field sampling design used a spatially stratified method to distribute the sampling locations at several water depth intervals within and near the river plumes; 54 samples were collected (Fig. 1). The sample points were distributed along five transects and sample locations were slightly shifted due to the conditions present on each sampling date. The water depths of 27 sampling locations were measured by a Vexilar® Hand-held Depth Sonar during the cruise on May 7, 2015. The depths of the earlier sampling locations were generated from bathymetry contours downloaded from Michigan Geographic Data Library (MiGDL). These generated depths have been verified by the 2015 field depth measures with a mean error of less than 10%.

Surface water samples and *in situ* spectral data were collected in parallel at each sampling location. Water samples collected were

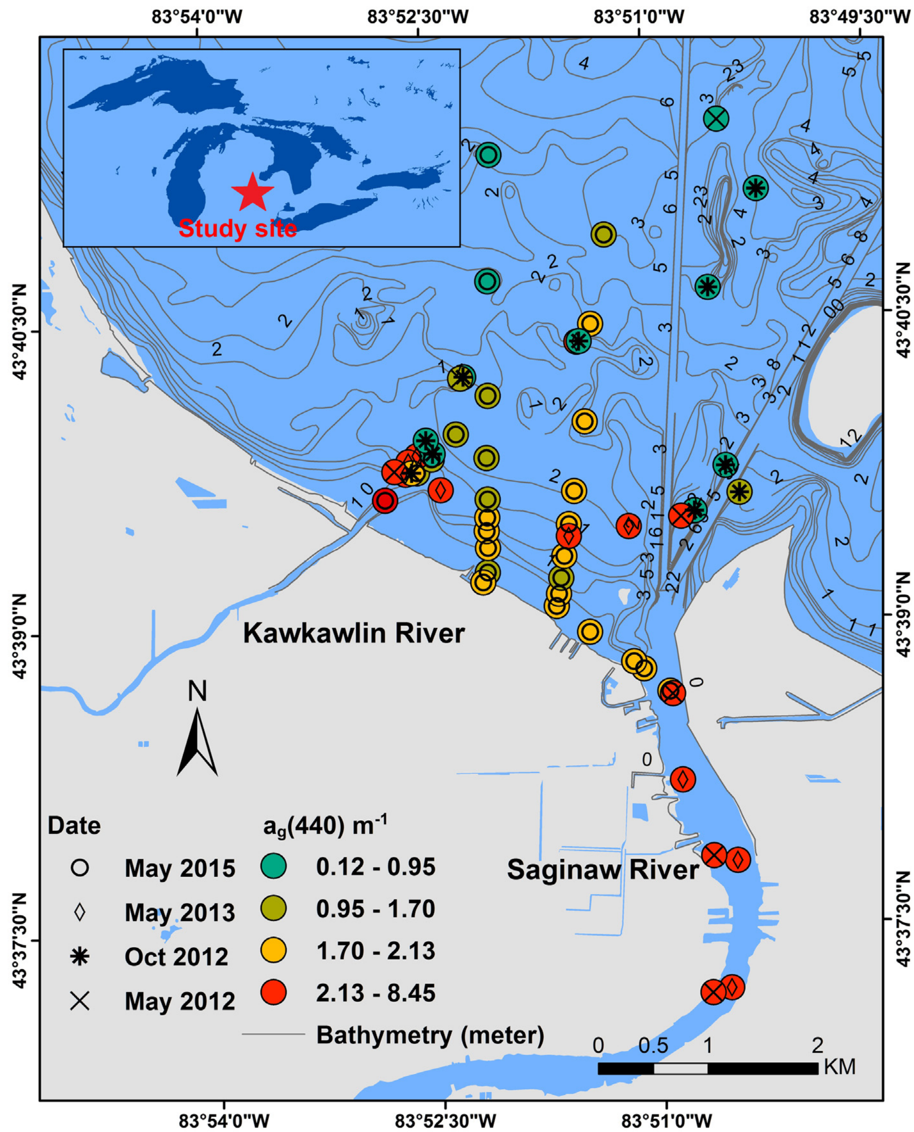

Fig. 1. The 54 samples located in the Saginaw River, Kawkawlin River, Saginaw Bay, and Lake Huron. The four field cruises were conducted from May 2012 to May 2015.

stored in amber bottles (polypropylene 500 ml) and kept chilled in a cooler until laboratory measurements of CDOM levels were performed. Samples at 5 locations were replicated for sampling uncertainty assessment (mean error < 3%). The *in situ* spectral data were collected at 2 m above the water surface with a Satlantic® HyperSAS and HyperOCR sensors. The cruises were arranged during cloud free weather and under ~2–8 m/s wind speed so that wave effect is minimum. The HyperSAS instrument was deployed by following the operation instructions to ensure sensor view angles were adjusted according to the solar position during above-surface spectra data measurements. The *in situ* spectral data included sky radiance (L_s), total upwelling radiance (L_t) and downwelling irradiance (E_d) from 400 nm to 800 nm. The radiance sensor for measuring L_t was pointed to the water surface at an angle of 40° from nadir. The radiance sensor for measuring L_s was pointed skyward with an angle of 40° from solar zenith. Both sensors were set at the angle of 90° from solar azimuth angle. The E_d irradiance sensor was mounted separately and perpendicularly to the water surface. At least 20 radiance/irradiance measures were recorded at each location. The averages of these 20 spectral curves were used for all further analyses.

In situ below-surface spectral data were measured to observe the water column light field. The below-surface upwelling irradiance was logged via a ASD® Fieldspec equipped with an underwater cosine corrected receptor. These below-surface spectra across 300–1000 nm were collected at 6 locations with varied depths (from ~0.6 m to ~4 m). These below-surface measurements were conducted vertically from just below the water surface to just above the bottom sediments at 0.3 m interval. All spectral measurements were carried out between 10 A.M. and 2 P.M. in cloud free weather and wind conditions ranged from ~2–4 m/s (2–8 knots) that were associated with waves ranging from 0.15 to 0.45 m according to the data from the National Weather Service. Other environment conditions did not vary significantly during the field measurements (depth, sediments, etc.).

The CDOM measurements for all the collected water samples were completed within six hours of collection. The water samples were first filtered using glass microfiber filters GF/F (nominal 0.7 μm pore size) according to the standard laboratory measurement of CDOM (Mannino et al., 2008; Vodacek et al., 1997). Then the filtrate was transferred into 0.01 m cuvettes to measure CDOM absorbance $A(\lambda)$ via a Cary® 60 UV–Vis Spectrophotometer with

Milli-Q water as blank. The CDOM absorption coefficient $a_g(\lambda)$ was calculated from Eq. (1):

$$a_g(\lambda) = \frac{\ln(10)}{L} \times A(\lambda) = 230.3 \times A(\lambda) \quad (1)$$

where L is the diameter of cuvette in meters. All laboratory measurements were performed in triplicate and averaged in order to increase overall accuracy.

The remote sensing reflectance R_{rs} was calculated from *in situ* spectral radiances and irradiance by

$$R_{rs} = \frac{L_t - \phi L_s}{E_d} \quad (2)$$

where E_d is downwelling irradiance, L_s is sky radiance, L_t is total upwelling radiance and ϕ is a proportionality factor that relates the L_s to water-surface reflected radiance, set as 0.028 (Mobley, 1999). Then just below-surface remote sensing reflectance (r_{rs}) was derived from R_{rs} as (Lee et al., 1998):

$$r_{rs}(\lambda) = \frac{R_{rs}(\lambda)}{0.52 + 1.7R_{rs}(\lambda)} \quad (3)$$

2.3. Shallow water bio-optical properties (SBOP) algorithm

A shallow water bio-optical properties algorithm (SBOP) was developed for CDOM absorption retrieval to reduce the uncertainty caused by bottom sediments. In optically shallow waters, the water-leaving reflectance is made up of contributions from both waterbody and bottom sediments. So the below-surface remote sensing reflectance r_{rs} can be modeled as (Lee et al., 2007):

$$r_{rs} = r_{rs}^c + r_{rs}^b = r_{rs}^{dp}(1 - e^{-D_c(a_t+b_b)H}) + \frac{1}{\pi}\rho e^{-D_b(a_t+b_b)H} \quad (4)$$

where r_{rs}^c represents the water column contribution. r_{rs}^b represents the bottom sediments contribution. $D(a_t + b_b)$ represents the light attenuation caused by water column absorption and backscattering for water column light components (D_c) or light components from bottom (D_b). Finally, D_c and D_b are empirical factors associated with under-water photon path elongation due to scattering and can be calculated as below (Lee et al., 1999):

$$D_c = 1.03\left(1 + 2.4\frac{b_b}{a_t + b_b}\right)^{0.5} \quad (5)$$

$$D_b = 1.05\left(1 + 5.5\frac{b_b}{a_t + b_b}\right)^{0.5} \quad (6)$$

The value 1.05 and 5.5 used in the calculation were determined after repeated experiments and they were found to be the optimal. r_{rs}^{dp} represents below-surface remote sensing reflectance when the water is infinitely deep and can be modeled as (Lee et al., 2013):

$$r_{rs}^{dp} = \left(0.089 + 0.125\frac{b_b}{a_t + b_b}\right)\frac{b_b}{a_t + b_b} \quad (7)$$

Several previous studies as well as our model calibration results showed that using 0.089 and 0.125 for the calculation of r_{rs}^{dp} would improve model applicability to shallow waters (open waters, coastal waters, and inland waters) (Barnes et al., 2013; Lee et al., 2009, 2013; Yang et al., 2013; Zhu and Yu, 2013). Then r_{rs} can be determined by the following bio-optical variables: bottom reflectance ρ, water depth H, absorption and backscattering coefficients a_t and b_b. For the SBOP algorithm, the total absorption coefficients (a_t) at a given wavelength (λ) is modeled from three components:

$$a_t(\lambda) = a_w(\lambda) + a_p(\lambda) + a_g(\lambda) \quad (8)$$

where $a_w(\lambda)$ is the pure water absorption coefficient, $a_g(\lambda)$ is the CDOM absorption coefficient, and $a_p(\lambda)$ represents the particle absorption coefficient, which include both phytoplankton and non-algal particles. The total backscattering coefficients $b_b(\lambda)$ is calculated via two components:

$$b_b(\lambda) = b_{bw}(\lambda) + b_{bp}(\lambda) \quad (9)$$

where $b_{bw}(\lambda)$ and $b_{bp}(\lambda)$ are backscattering coefficients of pure water and particles, respectively. The values of $a_w(\lambda)$ and $b_{bw}(\lambda)$ are known (Morel, 1974; Pope and Fry, 1997). The $b_{bp}(\lambda)$ and $a_g(\lambda)$ were modeled as follows (Lee et al., 2013):

$$b_{bp}(\lambda) = P\left(\frac{\lambda}{555}\right)^y \quad (10)$$

$$a_g(\lambda) = Me^{-S(\lambda-440)} \quad (11)$$

where y is the spectral parameter that determines the scattering decay and was estimated as (Lee et al., 2002):

$$y = 2\left(1 - 1.2e^{-0.9\frac{R_{rs}(444)}{R_{rs}(555)}}\right) \quad (12)$$

S is the parameter establishing the absorption decay slope (spectral slope) and its value is approximately 0.015 as derived from the global average value (Zhu et al., 2014). This value is more applicable to a broad range of water cases and reduces the bias in algorithm comparison. The unknown factor M is the CDOM absorption coefficient at 440 nm. P is the particle backscattering coefficient at 555 nm. There is a good positive correlation between $a_p(\lambda)$ and $b_{bp}(\lambda)$ as both are associated with suspended particulate matter (Babin et al., 2003; Zhu et al., 2014). Ultimately, $a_p(\lambda)$ was modeled as:

$$a_p(\lambda) = qP\left(\frac{\lambda}{555}\right)^y \quad (13)$$

where q = 0.75 which represents the empirical ratio of a_p and b_{bp} (Zhu and Yu, 2013; Zhu et al., 2013b). The bottom reflectance ($\rho(\lambda)$) at each wavelength is expressed as:

$$\rho(\lambda) = B\rho_{bottom}(\lambda) \quad (14)$$

where $\rho_{bottom}(\lambda)$ is the dominant bottom material spectrum (sand) and it is normalized by the reflectance at 555 nm (Lee et al., 2007). The B is an unknown factor which represents the bottom reflectance at 555 nm. A sensitivity analysis was conducted in order to confirm that global values are suitable for the relevant parameters (Table 1). Overall, using alternative settings has a negligible effect on the results compared to general setting. The general

Table 1
Sensitivity analysis of the algorithm parameters.

Parameters	General setting	Alternative setting	Accuracy change
$D_b = 1.05\left(1 + 5.5\frac{b_b}{a_t+b_b}\right)^{0.5}$	1.05, 5.5 New version HOPE	1.04, 5.4 Old version HOPE	+0.5%
$r_{rs}^{dp} = \left(0.089 + 0.125\frac{b_b}{a_t+b_b}\right)\frac{b_b}{a_t+b_b}$	0.089, 0.125 General water	0.084, 0.17 High scattering water	+2.5%
Spectral slope S	0.015 Global mean	0.0152 Field data-based	−0.5%

setting is preferable as algorithm validation is dependent less upon the study site.

Through Eqs. (4)–(14), r_{rs} is constructed to describe optically shallow waters' bio-optical properties and contains four unknown variables B, M, P and H:

$$r_{rs}(\lambda) = f(B, M, P, H)(\lambda) \tag{15}$$

The SBOP algorithm solves for these four unknown variables via spectral optimization. In the SBOP processing, the initial values of the B, M, P and H were set as following (Lee et al., 2013):

$$B = 0.1 \tag{16}$$

$$M = 0.075\left(\frac{R_{rs}(444)}{R_{rs}(555)}\right)^{-1.7} \tag{17}$$

$$P = 0.025\left(\frac{R_{rs}(444)}{R_{rs}(555)}\right)^{-1.7} \tag{18}$$

$$H = 1.5 \tag{19}$$

B, bottom reflectance at 555 nm, was set as 0.1. H, the average depth was set as 1.5 m according to study site conditions. After tests these initial values were found to be the best. Our optimization process minimizes the differences between modeled below-surface reflectance $\widehat{r_{rs}}$ and measured below-surface reflectance $r_{rs}(\lambda)$ (obtained from *in situ* spectral measurements or remote sensing images), ultimately determining each variable in order to derive CDOM absorption and bottom contribution. Specifically, the optimization aims to find these four variables that minimize the following error function:

$$err = \frac{\sqrt{\sum_{i=1}^{N}\left(r_{rs}(\lambda_i) - \widehat{r_{rs}}(\lambda_i)\right)^2}}{\sqrt{\sum_{i=1}^{N} r_{rs}(\lambda_i)}} \tag{20}$$

The nonlinear system solver function in Matlab was applied in this study, which used the trust region dogleg algorithm to process the optimization (Powell, 1968). The SBOP algorithm requires a minimum of four r_{rs} values at different wavelengths as input. So potentially it can be applied to both multispectral and hyperspectral data. In this study, the hyperspectral data (120 r_{rs} bands) was applied to estimate the CDOM absorption. The algorithm performance was evaluated by comparing remote sensing derived CDOM results with laboratory measurements of CDOM using field water samples. The following five statistical metrics were assessed: *bias*, mean normalized bias (MNB), absolute mean error (AME), root mean squared error (RMSE, log space) and R^2 (regression, Type II).

2.4. Adaptive approach for computation efficiency

In estimating CDOM in inland and coastal waters, a single scene of satellite data often contains a broad range of water depths (e.g. Landsat 8). The estimation of CDOM through the SBOP algorithm is generally both time and computation intensive, for the relatively complex equations illustrated above need to be solved through optimization. One way to improve optimization efficiency is to separate the water spectral data into high or low bottom effect groups and only apply SBOP to the high bottom effect (optically shallow) group. We introduce an adaptive approach of applying the SBOP algorithm only to optically shallow waters and applying the deep water semi-analytical algorithm (QAA-CDOM) to optically deep waters.

The QAA-CDOM is a representative semi-analytical algorithm for CDOM retrieval in deep waters (Zhu et al., 2014). This algorithm can be efficiently applied to a wide range of water conditions, including estuarine and coastal waters assuming the water is optically deep. It calculates CDOM absorption directly from R_{rs} in 13 steps. The first ten steps derive the total absorption coefficient $a_t(440)$ and $b_{bp}(555)$ (Lee et al., 2002; Zhu et al., 2013a). Then last three steps derive the absorption of particulates $a_p(440)$ from $b_{bp}(555)$ in order to calculate $a_g(440)$ by the following equations:

$$a_p(\lambda) = J_1 b_{bp}(555)^{J_2} \tag{21}$$

$$a_g(440) = a_t(440) - a_w(440) - a_p(440) \tag{22}$$

where $J_1 = 0.63$ and $J_2 = 0.88$ are two parameters that were estimated from *in situ* data from inland waters (Zhu and Yu, 2013). The required inputs of the QAA-CDOM algorithm are R_{rs} at wavelengths of 440, 490, 555 and 640 nm.

Water depth is a key factor determining the bottom effect and is often used to separate optically deep or optically shallow waters. However, the bottom effect is also highly influenced by water column attenuation (Barnes et al., 2014; Zhao et al., 2013). A tangible example is that bottom reflectance could contribute significantly to water-leaving radiance for deep but clear/transparent water with a highly reflective bottom such as sand. Therefore, the bottom effect index (BEI) was introduced which considers both the bathymetry and water column attenuation to quickly identify waters for which bottom reflectance is significant. It is defined as an exponential function because it has been established that underwater light is exponentially attenuated with water depth (Markager and Vincent, 2000):

$$BEI = e^{-\left(\frac{R_{rs}(\lambda_1)}{R_{rs}(\lambda_2)}\right)H} \tag{23}$$

where H is the water depth. The R_{rs} band ratio (e.g. 690/555 nm) represents light attenuation by the water column and was often used as a proxy for water turbidity in previous research (Dall'Olmo et al., 2005; Dogliotti et al., 2015; Doxaran et al., 2005, 2002). The ratio 690/555 nm was applied in this study.

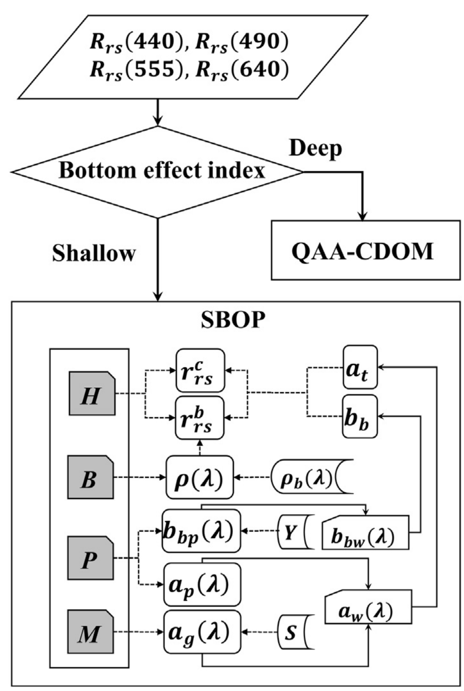

Fig. 2. Conceptual flowchart of adaptive approach and SBOP algorithm. In the SBOP algorithm, the H, B, P, and M were four unknown factors which were derived from optimization. The depth H affected the water column reflectance (r^c_{rs}) and bottom reflectance (r^b_{rs}). The bottom reflectance B contributed to the below-surface remote sensing reflectance r_{rs}. The CDOM absorption M and the particle backscattering P determined the light attenuation ($a_t + b_b$).

The adaptive approach applies either the SBOP or QAA-CDOM algorithm for individual location/spectra depending on the significance of bottom effect (Fig. 2). Initially, the field spectral data is subjected to the BEI in order to determine whether the waters are categorized as optically shallow or optically deep waters. Then, the optically shallow waters are processed via SBOP while the optically deep waters are processed by QAA-CDOM to estimate the CDOM absorption. This adaptive approach aims to improve the computation efficiency for the regions with known bathymetry data (e.g. the Great Lakes regions), which are largely available for near-coastal shallow waters. Alternatively, for multi-temporal CDOM monitoring, the bathymetry of the site can be derived from SBOP algorithm once, and then be applied for other seasons when using the adaptive approach.

3. Results and discussions

3.1. Spatial and seasonal variation of CDOM from field observation

Field water samples showed that CDOM levels exhibit a distinct spatial trend, descending from the near-shore lower river channel and river plume regions to the inner bay. The sampled CDOM absorption $a_g(440)$ widely ranged from 0.12 m^{-1} to 8.46 m^{-1} (Fig. 1). CDOM levels at the river sample locations were generally high, with the Saginaw River having a value as high as 8.45 m^{-1}. The average of CDOM levels around the plume area of the Kawkawlin River (5.38 m^{-1}) is much higher than that of the Saginaw River (1.73 m^{-1}). This marked difference was attributed to the terrestrial ecology of the drainage watersheds. The large proportion of both deciduous forest and associated litter and wetland areas within the Kawkawlin River watershed likely caused the higher CDOM levels in its plume area. The field sampling generally captured the complex spatial variation of CDOM in this area and provided a good foundation for evaluating these remote sensing algorithms.

Distinct seasonal variations of freshwater CDOM between May and October were also observed, likely driven by the organic carbon supply in the drainage watersheds and hydrological processes (Tian et al., 2013). The mean CDOM absorption of samples collected in May was 2.75 m^{-1}, much higher than that in October (mean value of 0.54 m^{-1}). The higher CDOM levels during the spring season are analogous to trends reported in a recent study, which reported that the surface and subsurface hydrology associated with snow melt is responsible for transporting organic matters from soil organic carbon pools into the river systems (Tian et al., 2013). Similarly, the Saginaw River watershed is dominated by the agricultural land use which has increased metabolic activities on crop residues in the spring (Spedding et al., 2004). The second most dominant land cover in the Saginaw River watershed is deciduous forest. The large proportion of soil carbon originates from the biological decay of both crop litters and forest leaf litters, so the soil carbon levels are much higher in spring when the large accumulation of carbon is flushed out of the soil through snowmelt. Meanwhile, the consumption of organic matters throughout the growing season leads to relatively lower soil carbon levels in October (Kalbitz et al., 2000).

These seasonal hydrological processes also explain inter-annual CDOM variability (Berto et al., 2010; Raymond and Oh, 2007). The sampled CDOM level in May 2015 was clearly lower (mean 2.05 m^{-1}) than that in 2013 (mean 3.51 m^{-1}) and 2012 (mean 3.70 m^{-1}). The winter of 2014–15 had relatively large snowfall accumulations and peak snowmelt occurred in April, much earlier than in 2012 and 2013 (Fig. 3). The available soil organic matter in the watersheds was largely depleted during this early spring thaw in mid-April 2015, which likely resulted in the observed lower CDOM levels during the May 2015 sampling campaign. Contrarily, the relatively higher CDOM levels sampled in May 2012 and 2013 were associated with the receding leg of a more normal spring discharge event.

Above-surface R_{rs} measured by the HyperSAS spectrometer demonstrated the potential of using remote sensing for the estimation of CDOM levels and other bio-optical properties of water. Fig. 4 illustrates how R_{rs} measured via HyperSAS is spectrally contaminated by strong bottom reflectance. The 27 samples on turbidity measurements (Secchi disk depth) were collected in May 2015 and were accompanied with comparable measurements of CDOM levels. All the spectra data in Fig. 4 were under the same general water turbidity conditions. The light attenuations by the water column were generally the same in these sites, but did differ with depth. The shallow water samples (0.6 m < Depth < 0.9 m) show reflectance (R_{rs}) twice as high as that of the deep water

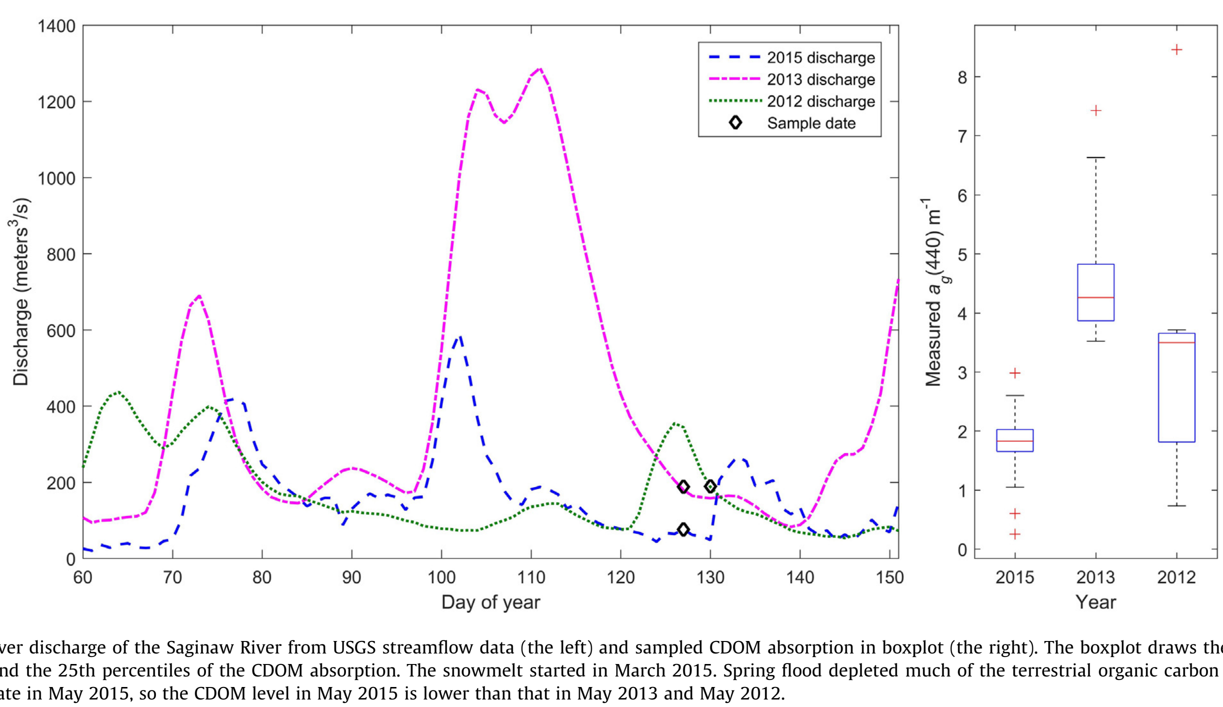

Fig. 3. River discharge of the Saginaw River from USGS streamflow data (the left) and sampled CDOM absorption in boxplot (the right). The boxplot draws the 75th, the median and the 25th percentiles of the CDOM absorption. The snowmelt started in March 2015. Spring flood depleted much of the terrestrial organic carbon before the sample date in May 2015, so the CDOM level in May 2015 is lower than that in May 2013 and May 2012.

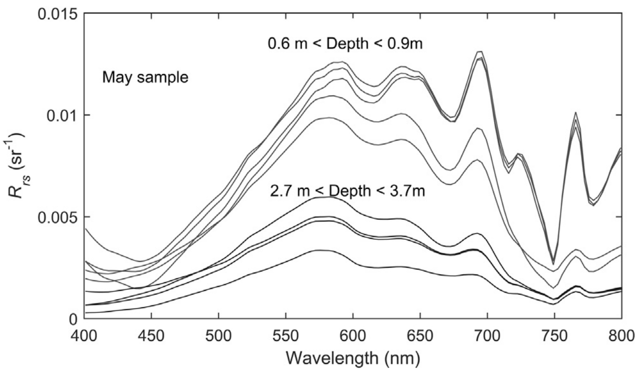

Fig. 4. The measured remote sensing reflectance at shallow (0.6 m < depth < 0.9 m) and deep (2.7 m < depth < 3.7 m) waters with similar CDOM absorption (1.8^{-1} < $a_g(440)$ < 2.3 m^{-1}) and turbidity in May 2015.

Table 2
Validation of SBOP and comparison to the QAA-CDOM algorithm.

Method	RMSE	Bias	MNB	AME	R^2
QAA-CDOM	0.31	1.6129	0.8534	0.9343	0.48
SBOP	0.22	0.0701	0.3393	0.5441	0.74

samples (2.7 m < Depth < 3.7 m), which is attributed to the bottom sediments reflectance. Therefore, neglecting bottom reflectance could introduce significant uncertainties in CDOM retrieval for optically shallow waters. Higher bottom effect will lead directly to higher water-leaving radiance. Consequently, the prevailing deep waters CDOM retrieval algorithms would significantly overestimate CDOM levels (Zhu et al., 2013b). Therefore, our *in situ* spectra observations strongly suggest that bottom reflectance must be considered when applying CDOM retrieval algorithms for optically shallow waters.

3.2. Algorithm performance and validation of SBOP

We validated SBOP with laboratory measured CDOM from field water samples and assessed the algorithm performance in comparison to QAA-CDOM (Table 2). The SBOP algorithm performed better than QAA-CDOM with respect to all five error metrics. In particular, QAA-CDOM resulted in a much higher bias (1.6129). In the shallow waters, the high bottom reflectance significantly increases the reference at longer wavelengths, which leads to the high spectral slope of remote sensing reflectance (440–600 nm). Consequently, CDOM is overestimated in deep water algorithm QAA-CDOM. In contrast, the SBOP (bias = 0.0701) successfully modeled both the bottom and water column components of R_{rs} and greatly reduced the error and bias. Since over half of the sample sites were located in optically shallow waters, the performance of the QAA-CDOM algorithm was indeed affected by the intrusive bottom reflectance, whereas the SBOP algorithm successfully reduced uncertainty on CDOM retrieval for optically shallow waters. The SBOP algorithm dramatically improves the accuracy of CDOM estimation in optically shallow freshwater environments.

The remote sensing derived $a_g(440)$ vs. ground truth $a_g(440)$ for individual samples is shown in Fig. 5. The overall R^2 of SBOP (R^2 = 0.74) significantly outperformed QAA-CDOM (R^2 = 0.48). The SBOP performs significantly better by taking into consideration the bottom reflectance in the shallow water regions (labeled as Group B and Group C). Furthermore, the error range resulting from the QAA-CDOM algorithm was also larger and some samples have estimated CDOM (between ~10 m^{-1} and ~14 m^{-1}) two or three times larger than the measured values. These overestimations were from samples located at the most shallow and clearer locations (less than 1 m) in the Saginaw River and near shore regions where ground-truthed CDOM levels were relatively low (labeled as group B). These results further confirmed that neglecting bottom reflectance does indeed result in much higher algorithm uncertainty. Comparatively, the QAA-CDOM algorithm produced more accurate CDOM estimation for samples in shallow waters that had relatively high CDOM levels (between ~4 m^{-1} and ~8 m^{-1}) (labeled as group C). This scenario occurred in the Kawkawlin River plume regions where water color was stained brown resulting from its watershed being dominated by deciduous forest (leaf litters) and wetland. In essence, high CDOM levels and associated strong water column absorption reduced the overall negative influence of the bottom effect. CDOM levels of deep water samples labeled as group A were slightly underestimated by the SBOP

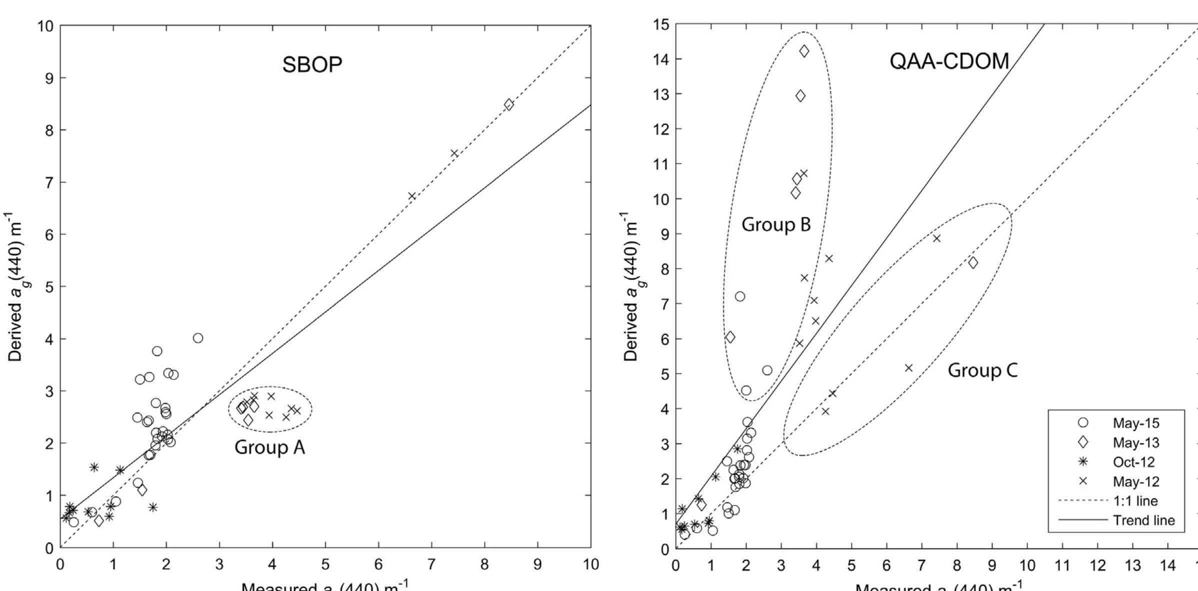

Fig. 5. The measured vs. derived $a_g(440)$ from SBOP (the left) and QAA-CDOM (the right) algorithm. Group B represents the shallow water samples (<1 m) with low CDOM levels (between ~1.8 m^{-1} to ~3.5 m^{-1}). Group C represents the shallow water samples (<1 m) with high CDOM levels (between ~4 m^{-1} and ~8 m^{-1}). Group A is the deep water samples (>1.5 m).

algorithm. This is caused by the over-estimation of bottom reflectance for deep water samples, as the trend line deviated from the 45 degree 1:1 line. However, the performance of both algorithms degraded when the CDOM level is very low. Specifically, low CDOM samples collected in May 2015 have relatively larger errors.

3.3. Bottom contribution effect on SBOP algorithm uncertainty

The ASD measured spectra within the water column at six selected locations were assessed to study the relative role of bottom effect and to examine the SBOP algorithm's overall effectiveness. Fig. 6 is an example of the differences in the remote sensing reflectance at three levels of water depths: just below water surface, just above bottom, and at mid depth measured with ASD Fieldspec. Remote sensing reflectance decreases with measurement depth due to absorption and scattering in the optical transmission processes. We choose two measured variables, just below surface reflectance (r_{rs}) and just above bottom sediments reflectance (ρ) at 555 nm to be compared to their estimated values by SBOP. Fig. 7 compared these ASD measured values and the SBOP estimated r_{rs} and ρ. The R^2 value was 0.89 for $r_{rs}(555)$ and 0.79 for ρ (555). These relatively high correlations demonstrate that SBOP reasonably modeled water optical properties with a bottom reflectance effect. This deviation is understandable since r_{rs} and B were solved via optimization with 54 total samples/locations. The relative error of SBOP modeled $r_{rs}(555)$ and $B(555)$ were displayed for different depths (Fig. 7c). The algorithm generally performs well at shallow to moderate depths (∼1 m to ∼2.5 m). In these regions the bottom contributions account for a relatively lower percentage of total water leaving reflectance (∼15%) when compared to the extremely shallow water sites (∼30%). The large percentage of the bottom contribution in extremely shallow waters (<1 m) does indeed lead to relatively high errors. Overall, the errors are smaller in optically shallow waters than optically deep waters. The implication might be that the set of parameters (determined by optimization) describe the light field of the well-mixed water columns in these near-shore waters better, but introduces increasing errors as water depth increases lead to absorption and scattering.

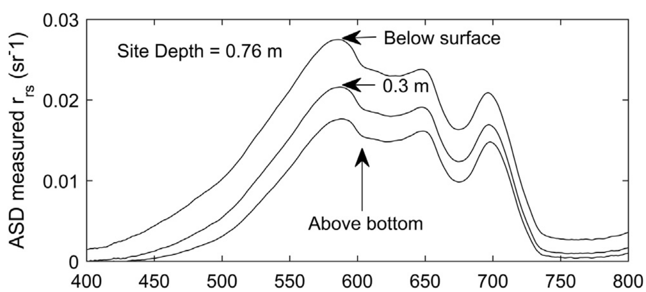

Fig. 6. The below surface remote sensing reflectance was measured by the ASD Fieldspec from just below the water surface to just above the bottom. The plot showed the spectral results on shallow (0.76 m) site.

We plotted percent error with regard to depth or bottom effect index (BEI) at individual sampling sites, to investigate the influence of bottom effect on algorithm performance of the optically shallow water algorithm (SBOP) and the optically deep water semi-analytical algorithm (QAA-CDOM) (Fig. 8). Such comparisons help to determine the threshold for the optically deep and optically shallow waters at our study site. At a depth <1.5 m, the SBOP generated a reasonably small error (MNB = 0.0915, R^2 = 0.67) while the QAA-CDOM algorithm significantly over-estimates CDOM levels. The MNB (1.2007) and R^2 (0.24) indicated that the QAA-CDOM caused very large uncertainty in such shallow waters (Table 3, Fig. 9). Similarly, in waters with high bottom effect (BEI ≥ 0.2), the SBOP (RMSE = 0.16, R^2 = 0.75) generates more reasonable results compared to the QAA-CDOM (RMSE = 0.32, R^2 = 0.30). Conversely, in the waters with negligible bottom effect (BEI < 0.2) the QAA-CDOM results in a slightly lower RMSE and higher R^2 than

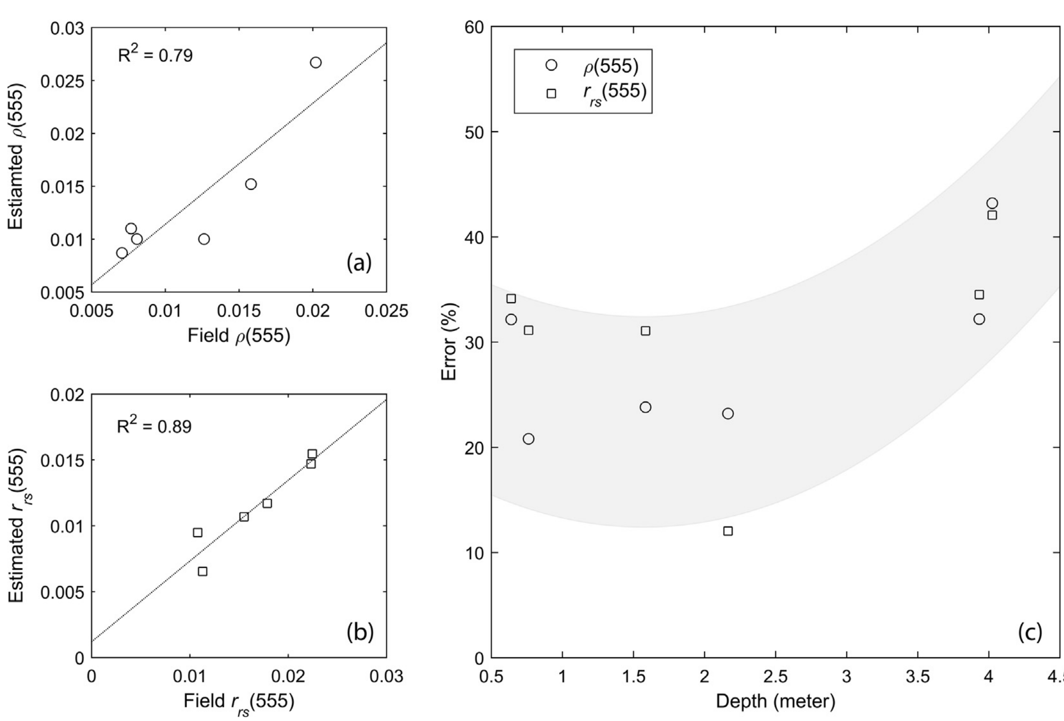

Fig. 7. Comparisons of ASD measured reflectance and SBOP modeled just above the bottom (a) and just below the surface (b) reflectance. The relative errors of below surface remote sensing reflectance (r_{rs}) and bottom reflectance (ρ) at 555 nm were assessed at six different locations (c). The shaded area indicates the error trend of the SBOP. The maximum of the error was calculated to be the shade area boundary.

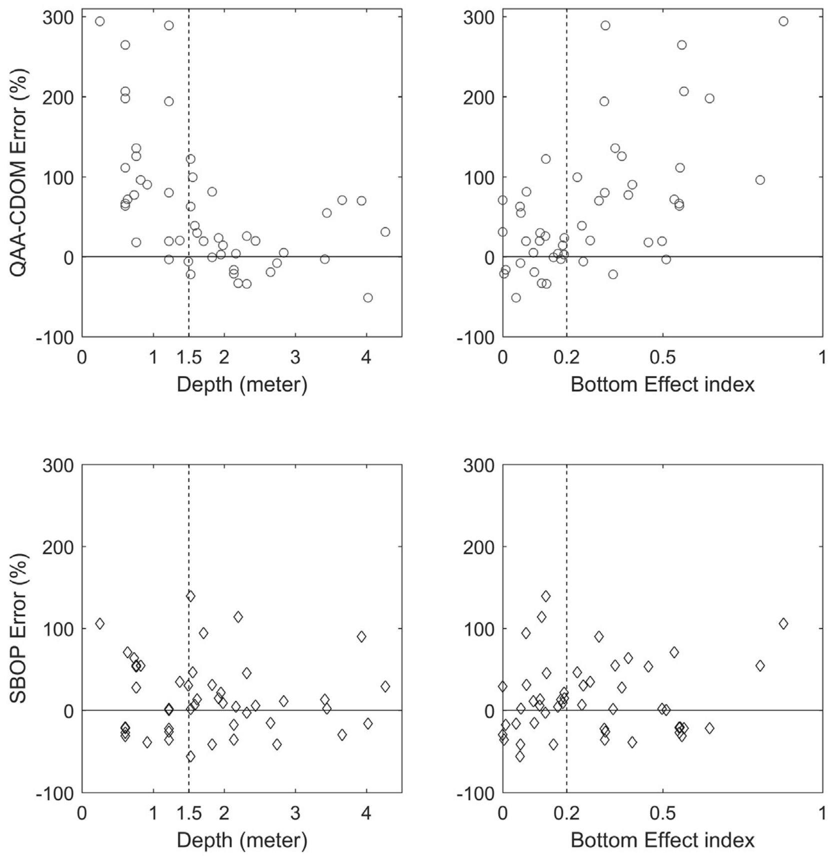

Fig. 8. The percent errors of CDOM estimation from QAA-CDOM and SBOP methods related to depth and bottom effect index. When depth < 1.5 m or BEI > 0.2, the QAA-CDOM outputs high error results.

Table 3
Validations of QAA-CDOM and SBOP for optically shallow and deep groups when applying Depth or BEI threshold for separation.

Method	RMSE	Bias	MNB	AME	R^2	Optically depth
QAA-CDOM	0.26	0.2488	0.5913	0.7219	0.80	*Depth* > *1.5* m
SBOP	0.26	0.1418	0.5144	0.6749	0.72	*Depth* > *1.5* m
QAA-CDOM	0.35	3.5169	1.1922	1.2007	0.24	*Depth* ≤ *1.5* m
SBOP	0.16	−0.0326	0.0915	0.3607	0.67	*Depth* ≤ *1.5* m
QAA-CDOM	0.26	0.2551	0.6102	0.7038	0.81	*BEI < 0.2*
SBOP	0.27	0.1186	0.5182	0.6842	0.47	*BEI < 0.2*
QAA-CDOM	0.32	2.9375	0.9819	1.0481	0.30	*BEI ≥ 0.2*
SBOP	0.16	0.0330	0.1494	0.3761	0.75	*BEI ≥ 0.2*

SBOP (QAA-CDOM: RMSE = 0.26, R^2 = 0.81; SBOP: RMSE = 0.27, R^2 = 0.47). CDOM levels were under-estimated by SBOP compared to the QAA-CDOM where the bottom effect was low (Fig. 9). As water depth increases, the light is strongly attenuated by the water column and its constituents in both the downward and upward paths. Theoretically, at a certain depth, bottom reflectance contributed no light to the total water leaving radiance (Dogliotti et al., 2015). However, the SBOP output does indicate a minimal bottom contribution to the total water leaving radiance at these relatively high depths, which inherently over-emphasizes the bottom contribution and consequently underestimates the water column contribution. The constraints of *B* was set to the range of $0.01 \leqslant B \leqslant 0.9$. After the optimization, the minimal *B* was approximately 0.05 for the optically deep waters. The SBOP algorithm does not produce a *B* constraint for the non-bottom effect waters. This might explain why SBOP outputs slightly under-estimation for the optically deep waters. This limitation of the SBOP algorithm creates the need to choose the more suited CDOM retrieval algorithm (QAA-CDOM and SBOP) for waters with low bottom effect or high bottom effect respectively.

3.4. The bottom effect adaptive approach

Adaptive approach improves the CDOM retrieval accuracy and saves computation time by applying the most suitable algorithm according to the amount of bottom effect (i.e., SBOP for optically shallow waters and QAA-CDOM for optically deep waters). It overcomes the limits of each individual algorithm and considers bottom contribution only when necessary. We examined both water depth and BEI as a metric used to classify optically deep vs. optically shallow waters. The thresholds were set as optically shallow waters (depth ≤ 1.5 m or BEI ≥ 0.2) and optically deep waters (depth > 1.5 m or BEI < 0.2). The threshold values were assessed through the comparisons of the algorithm performances. The BEI = 0.2 and depth = 1.5 m was generated through the performances of SBOP and QAA-CDOM algorithms (Fig. 8). These two

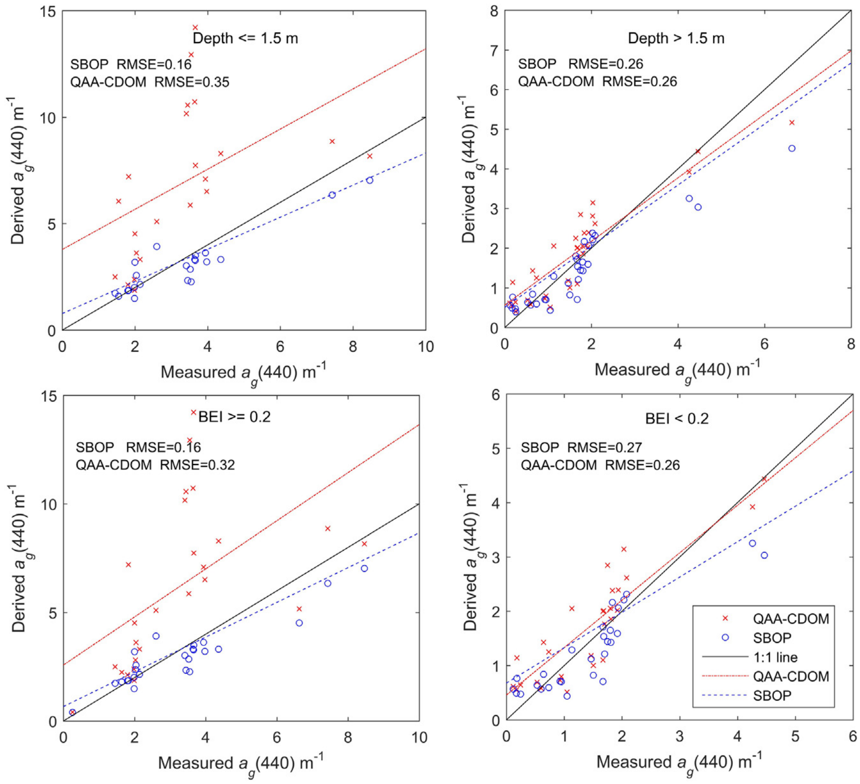

Fig. 9. Derived vs. measured $a_g(440)$ for optically shallow and deep groups when separated by the depth or BEI threshold. SBOP significantly outperforms QAA-CDOM in optically shallow waters (depth ≤ 1.5 m or BEI ≥ 0.2), while it slightly under-estimates for optically deep waters (depth > 1.5 m or BEI < 0.2).

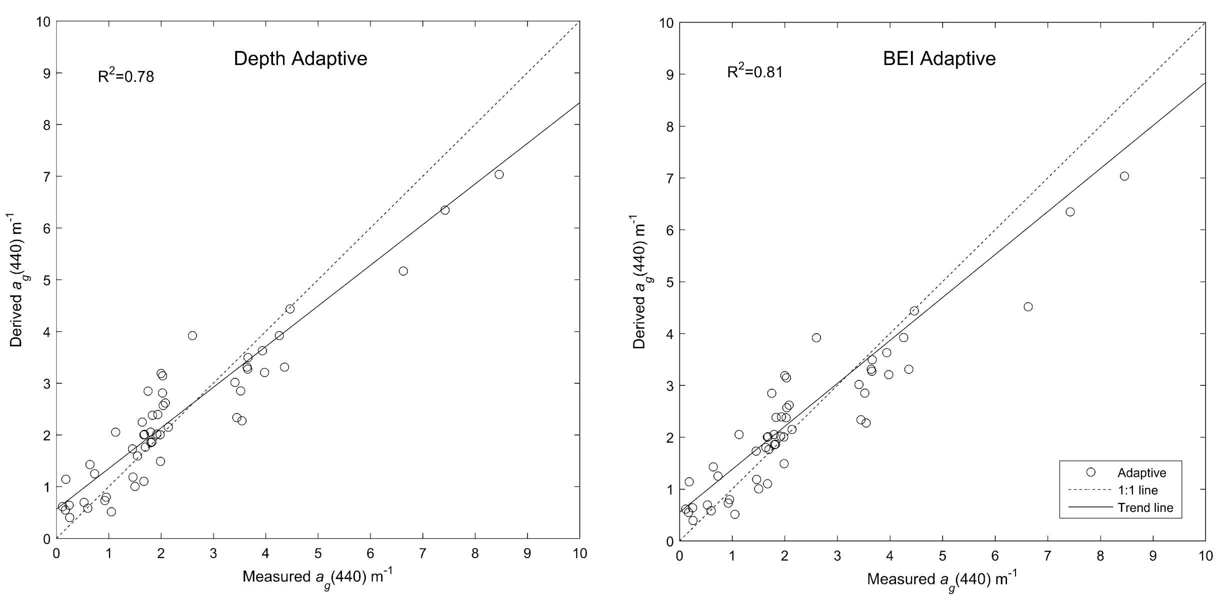

Fig. 10. Derived vs. measured $a_g(440)$ from Depth (the left) and BEI (the right) adaptive methods. The trend line resulted from BEI adaptive approach is closer to the 1:1 line and indicates a better overall performance.

threshold values also provide the most accuracy separation for the adaptive approach (optically deep waters used QAA-CDOM & optically shallow waters used SBOP). We tested multiple values to get these threshold values. The estimation results from the adaptive method are validated in Fig. 10 and Table 4. The BEI and depth adaptive methodologies can both utilize the advantages of the QAA-CDOM and SBOP algorithms to output reliable results (Tables 2 and 4). The performance evaluation shows that the BEI adaptive method (RMSE = 0.22 and R^2 = 0.81) has the advantage over the depth adaptive method (RMSE = 0.23 and R^2 = 0.78) (Table 4). The trend line of the BEI method is closer to the 45 degree 1:1 line at relatively high CDOM levels, indicating BEI introduces less bias for these high CDOM samples (Fig. 10). Due to the relatively lower number of samples with deep clear waters and high bottom effect, the performance of the BEI adaptive approach is not markedly 7better than the depth adaptive method. When one considers both

Table 4
The validations of Depth and BEI adaptive methods for $a_g(440)$ retrieval.

Method	RMSE	Bias	MNB	AME	R^2
Depth adaptive	0.23	0.1424	0.3931	0.5694	0.78
BEI adaptive	0.22	0.1523	0.3969	0.5521	0.81

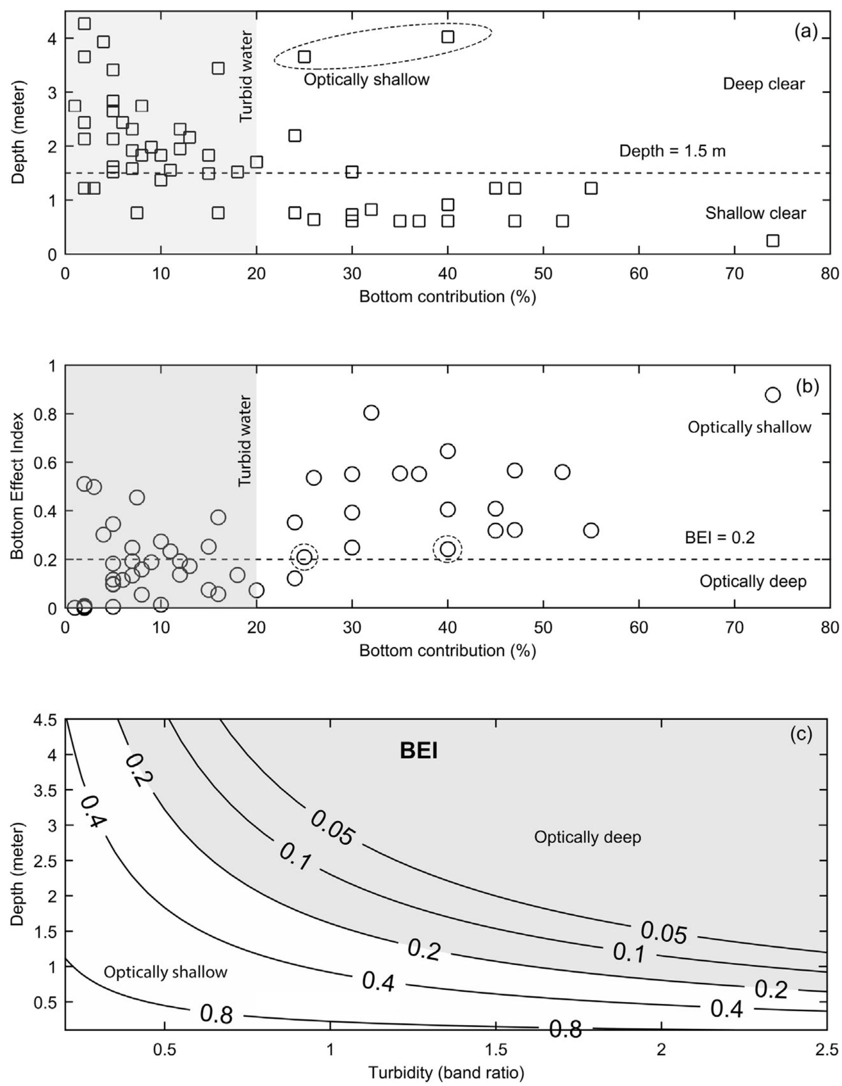

Fig. 11. The bottom contribution vs. depth (a) and bottom contribution vs. bottom effect index (b) for individual samples. The turbid water samples indicate that the bottom contributions are less than 20%. Two deep clear water samples with high bottom contribution were reasonably categorized as optically shallow water by the BEI method, different from using our Depth threshold. Panel c plots the BEI value as isolines as a function of the depth and turbidity. The BEI considers both the bathymetry and water column attenuation to separate the optically shallow and optically deep waters.

the computation efficient and accuracy, the adaptive approach is the suggested scheme to derive CDOM levels for inland freshwater and shallow coastal waters.

Our newly proposed BEI quickly separates optically shallow vs. optically deep waters based on both water depth and light attenuation (approximated by a band ratio) prior to the implementation of the adaptive method. In order to compare how well the two metrics, water depth and BEI, represent bottom effect, each was independently plotted relative to bottom contribution in Fig. 11a and b, respectively. Note that for this investigation, bottom contribution (BC) for each sample was calculated as the ratio of bottom reflectance (B) and below-surface reflectance (r_{rs}). In Fig. 11a and b, the shaded region represents a bottom contribution <20%, which referenced very turbid waters having low light penetration and negligible bottom effect. Bottom contribution >20% represents optically shallow waters, which theoretically not only include shallow water, but also some relatively deep clear water samples. Depth ranging from 0 to 4 m represents a gradient from optically shallow to optically deep waters. In contrast, a BEI index ranging from 1 to 0 represents a gradient from optically shallow to optically deep waters.

The depth metric cannot properly classify these clear deep or optically shallow waters (dashed circle in Fig. 11a). These samples lead to the high uncertainties in the depth adaptive approach since they were processed by QAA-CDOM without considering bottom reflectance. In contrast, BEI takes into account both water depth and column attenuation. The deep clear water samples circled in Fig. 11a (e.g. 4.2 m with the bottom contribution of 40%) were properly distinguished as high bottom contamination samples (with BEI > 0.2) in Fig. 11b. For the "deep clear water", the low turbidity waters have relatively low light attenuations, so even the physically deep waters have a high bottom effect. Therefore, these "deep clear water" locations should be classified as optically shallow waters. Fig. 11c presents the bottom effect index expressed as isolines as a function of the depth and turbidity (R_{rs} ratio). The BEI 0.2 isoline (shaded area) expresses the threshold between optically shallow and optically deep waters that effectively separates high/low bottom effect zones. High turbidity waters lead to high light attenuation which indicates a much lower amount of light was reflected upwards by the bottom, so only very shallow waters (less than 1 m) were classified as optically shallow waters. In contrast, the low turbidity waters have relatively low light attenuations, so even the deeper sample locations have a high bottom effect and should therefore be classified as optically shallow waters. Therefore, it is clear that utilizing the BEI metric leads to a more accurate adaptive approach than using our depth metric. Moreover, it can be easily derived and applied to many other aquatic remote sensing studies for fast identification of those areas where bottom reflectance influences CDOM measurements.

4. Conclusions

The optically shallow inland and coastal waters are important pathways for exporting terrestrially derived carbon sources into aquatic ecosystems. However, bottom reflectance introduces high uncertainty to the remote sensing estimation of water bio-optical properties (e.g. $a_g(440)$). In addition, for terrestrial carbon dominated freshwater environments, CDOM levels exhibit a very broad range (e.g. 0.12 m^{-1} to 8.46 m^{-1} in this study). These two characteristics present challenges for the remote sensing retrieval of freshwater biogeochemistry in the coastal and inland waters. Based on multi-date *in situ* measurements, this study developed an efficient shallow water CDOM estimation algorithm (SBOP). The overall performance evaluation (RMSE = 0.22 and $R^2 = 0.74$) demonstrated that the SBOP algorithm can be successfully applied to the optically shallow fresh waters with relatively homogeneous bottom sediments/conditions.

Ultimately, the SBOP model is uniquely designed for estimating CDOM absorption in optically shallow waters by taking into account the bottom reflectance component of total upwelling radiance. The SBOP algorithm significantly outperforms QAA-CDOM in these optically shallow waters (SBOP $R^2 = 0.74$ and QAA-CDOM $R^2 = 0.48$). In addition, the algorithm separately derives CDOM absorption as opposed to a combined absorption a_{dg} from prevailing ocean color algorithms. The removal of bottom effect from total radiance reduces the CDOM estimation uncertainty, and therefore extends effective carbon monitoring capabilities to optically shallow inland and coastal waters.

Widespread monitoring of water carbon from remote sensing data in the inland and coastal shallow waters demand the processing of large volumes of satellite data. We propose a BEI adaptive approach for algorithm selection. The BEI is designed to improve the computation efficiency for the regions having reliable bathymetry data, which are largely available for near-coastal and inland shallow waters. The BEI is able to quickly identify bottom contaminated water spectra/pixels based on both the bathymetry and water turbidity, so as to differentiate optically shallow waters. The BEI adaptive approach (BEI $R^2 = 0.81$) can efficiently as well as accurately aid in the selection of the proper algorithm for the estimation of water CDOM absorption.

In summary, our study investigated the potentials of remote sensing methods for capturing seasonal and spatial dynamics of CDOM in optically shallow water environments. Our newly developed SBOP algorithm offers a new inversion algorithm that directly considers bottom effect in radiative transfer equation. The BEI based adaptive approach presents a more efficient and fast method for monitoring terrigenous carbon export to inland and coastal waters with broad CDOM conditions. The outcome of this investigation will ultimately improve the monitoring of carbon pools and their transport gradients and mechanisms from terrestrial to aquatic systems at both regional and global scales.

Acknowledgement

This research is supported by two collaborative grants from the National Science Foundation (Grant #: 1025547; Grant #: 1230261) and one Faculty Research Grant at University of Massachusetts-Amherst.

References

Aitkenhead-Peterson, J., McDowell, W., Neff, J., Stuart, E., Robert, L., 2003. Sources, Production, and Regulation of Allochthonous Dissolved Organic Matter Inputs to Surface Waters. Academic Press, San Diego.

Babin, M., Stramski, D., Ferrari, G.M., Claustre, H., Bricaud, A., Obolensky, G., Hoepffner, N., 2003. Variations in the light absorption coefficients of phytoplankton, nonalgal particles, and dissolved organic matter in coastal waters around Europe. J. Geophys. Res. 108, 3211.

Barnes, B.B., Hu, C., Cannizzaro, J.P., Craig, S.E., Hallock, P., Jones, D.L., Lehrter, J.C., Melo, N., Schaeffer, B.A., Zepp, R., 2014. Estimation of diffuse attenuation of ultraviolet light in optically shallow Florida Keys waters from MODIS measurements. Remote Sens. Environ. 140, 519–532.

Barnes, B.B., Hu, C., Schaeffer, B.A., Lee, Z., Palandro, D.A., Lehrter, J.C., 2013. MODIS-derived spatiotemporal water clarity patterns in optically shallow Florida Keys waters: a new approach to remove bottom contamination. Remote Sens. Environ. 134, 377–391.

Battin, T.J., Luyssaert, S., Kaplan, L.A., Aufdenkampe, A.K., Richter, A., Tranvik, L.J., 2009. The boundless carbon cycle. Nat. Geosci. 2, 598–600.

Berto, D., Giani, M., Savelli, F., Centanni, E., Ferrari, C., Pavoni, B., 2010. Winter to spring variations of chromophoric dissolved organic matter in a temperate estuary (Po River, northern Adriatic Sea). Marine Environ. Res. 70, 73–81.

Brando, V.E., Anstee, J.M., Wettle, M., Dekker, A.G., Phinn, S.R., Roelfsema, C., 2009. A physics based retrieval and quality assessment of bathymetry from suboptimal hyperspectral data. Remote Sens. Environ. 113, 755–770.

Brando, V.E., Dekker, A.G., 2003. Satellite hyperspectral remote sensing for estimating estuarine and coastal water quality. Geosci. Remote Sens., IEEE Trans. 41, 1378–1387.

Brezonik, P.L., Olmanson, L.G., Finlay, J.C., Bauer, M.E., 2015. Factors affecting the measurement of CDOM by remote sensing of optically complex inland waters. Remote Sens. Environ. 157, 199–215.

Budhiman, S., Salama, M.S., Vekerdy, Z., Verhoef, W., 2012. Deriving optical properties of Mahakam Delta coastal waters, Indonesia using in situ measurements and ocean color model inversion. ISPRS J. Photogramm. Remote Sens. 68, 157–169.

Campbell, G., Phinn, S.R., Dekker, A.G., Brando, V.E., 2011. Remote sensing of water quality in an Australian tropical freshwater impoundment using matrix inversion and MERIS images. Remote Sens. Environ. 115, 2402–2414.

Carder, K., Chen, F., Cannizzaro, J., Campbell, J., Mitchell, B., 2004. Performance of the MODIS semi-analytical ocean color algorithm for chlorophyll-< i> a</i>. Adv. Space Res. 33, 1152–1159.

Cui, T., Zhang, J., Tang, J., Sathyendranath, S., Groom, S., Ma, Y., Zhao, W., Song, Q., 2014. Assessment of satellite ocean color products of MERIS, MODIS and SeaWiFS along the East China Coast (in the Yellow Sea and East China Sea). ISPRS J. Photogramm. Remote Sens. 87, 137–151.

Dall'Olmo, G., Gitelson, A.A., Rundquist, D.C., Leavitt, B., Barrow, T., Holz, J.C., 2005. Assessing the potential of SeaWiFS and MODIS for estimating chlorophyll concentration in turbid productive waters using red and near-infrared bands. Remote Sens. Environ. 96, 176–187.

Dekker, A.G., Phinn, S.R., Anstee, J., Bissett, P., Brando, V.E., Casey, B., Fearns, P., Hedley, J., Klonowski, W., Lee, Z.P., 2011. Intercomparison of shallow water bathymetry, hydro-optics, and benthos mapping techniques in Australian and Caribbean coastal environments. Limnol. Oceanogr.: Methods 9, 396–425.

Del Castillo, C.E., Coble, P.G., Morell, J.M., López, J.M., Corredor, J.E., 1999. Analysis of the optical properties of the Orinoco River plume by absorption and fluorescence spectroscopy. Mar. Chem. 66, 35–51.

Del Vecchio, R., Blough, N.V., 2004. Spatial and seasonal distribution of chromophoric dissolved organic matter and dissolved organic carbon in the Middle Atlantic Bight. Mar. Chem. 89, 169–187.

Dogliotti, A., Ruddick, K., Nechad, B., Doxaran, D., Knaeps, E., 2015. A single algorithm to retrieve turbidity from remotely-sensed data in all coastal and estuarine waters. Remote Sens. Environ. 156, 157–168.

Doxaran, D., Cherukuru, R., Lavender, S., 2005. Use of reflectance band ratios to estimate suspended and dissolved matter concentrations in estuarine waters. Int. J. Remote Sens. 26, 1763–1769.

Doxaran, D., Froidefond, J.-M., Castaing, P., 2002. A reflectance band ratio used to estimate suspended matter concentrations in sediment-dominated coastal waters. Int. J. Remote Sens. 23, 5079–5085.
Ferrari, G.M., Dowell, M.D., Grossi, S., Targa, C., 1996. Relationship between the optical properties of chromophoric dissolved organic matter and total concentration of dissolved organic carbon in the southern Baltic Sea region. Mar. Chem. 55, 299–316.
Giardino, C., Bresciani, M., Valentini, E., Gasperini, L., Bolpagni, R., Brando, V.E., 2015. Airborne hyperspectral data to assess suspended particulate matter and aquatic vegetation in a shallow and turbid lake. Remote Sens. Environ. 157, 48–57.
Hestir, E.L., Brando, V., Campbell, G., Dekker, A., Malthus, T., 2015. The relationship between dissolved organic matter absorption and dissolved organic carbon in reservoirs along a temperate to tropical gradient. Remote Sens. Environ. 156, 395–402.
Hoge, F.E., Lyon, P.E., 1996. Satellite retrieval of inherent optical properties by linear matrix inversion of oceanic radiance models: an analysis of model and radiance measurement errors. J. Geophys. Res. 101. 16631-16616,16648.
IPCC, 2007. Climate Change 2007: Impacts, Adaptation and Vulnerability: Working Group II Contribution to the Fourth Assessment Report of the IPCC Intergovernmental Panel on Climate Change. Cambridge University Press.
Kalbitz, K., Solinger, S., Park, J.-H., Michalzik, B., Matzner, E., 2000. Controls on the dynamics of dissolved organic matter in soils: a review. Soil Sci. 165, 277–304.
Klonowski, W.M., Fearns, P.R., Lynch, M.J., 2007. Retrieving key benthic cover types and bathymetry from hyperspectral imagery. J. Appl. Remote Sens. 1. 011505-011505-011521.
Kowalczuk, P., Cooper, W.J., Whitehead, R.F., Durako, M.J., Sheldon, W., 2003. Characterization of CDOM in an organic-rich river and surrounding coastal ocean in the South Atlantic Bight. Aquat. Sci. 65, 384–401.
Kutser, T., Pierson, D.C., Kallio, K.Y., Reinart, A., Sobek, S., 2005. Mapping lake CDOM by satellite remote sensing. Remote Sens. Environ. 94, 535–540.
Kutser, T., Verpoorter, C., Paavel, B., Tranvik, L.J., 2015. Estimating lake carbon fractions from remote sensing data. Remote Sens. Environ. 157, 138–146.
Lee, Z., 2006. Reports of the International Ocean-Colour Coordinating Group.
Lee, Z., Carder, K.L., Arnone, R.A., 2002. Deriving inherent optical properties from water color: a multiband quasi-analytical algorithm for optically deep waters. Appl. Opt. 41, 5755–5772.
Lee, Z., Carder, K.L., Mobley, C.D., Steward, R.G., Patch, J.S., 1998. Hyperspectral remote sensing for shallow waters. I. A semianalytical model. Appl. Opt. 37, 6329–6338.
Lee, Z., Carder, K.L., Mobley, C.D., Steward, R.G., Patch, J.S., 1999. Hyperspectral remote sensing for shallow waters. 2. Deriving bottom depths and water properties by optimization. Appl. Opt. 38, 3831–3843.
Lee, Z., Casey, B., Arnone, R., Weidemann, A., Parsons, R., Montes, M.J., Gao, B.-C., Goode, W., Davis, C., Dye, J., 2007. Water and bottom properties of a coastal environment derived from Hyperion data measured from the EO-1 spacecraft platform. J. Appl. Remote Sens. 1. 011502-011502-011516.
Lee, Z., Lubac, B., Werdell, J., Arnone, R., 2009. An update of the quasi-analytical algorithm (QAA_v5). IOCCG software report. <www.ioccg.org/groups/Software_OCA>.
Lee, Z., Weidemann, A., Arnone, R., 2013. Combined Effect of Reduced Band Number and Increased Bandwidth on Shallow Water Remote Sensing: The Case of WorldView 2.
Majozi, N.P., Salama, M.S., Bernard, S., Harper, D.M., Habte, M.G., 2014. Remote sensing of euphotic depth in shallow tropical inland waters of Lake Naivasha using MERIS data. Remote Sens. Environ. 148, 178–189.
Mannino, A., Russ, M.E., Hooker, S.B., 2008. Algorithm development and validation for satellite-derived distributions of DOC and CDOM in the US Middle Atlantic Bight. J. Geophys. Res.: Oceans (1978–2012) 113.
Maritorena, S., d'Andon, O.H.F., Mangin, A., Siegel, D.A., 2010. Merged satellite ocean color data products using a bio-optical model: characteristics, benefits and issues. Remote Sens. Environ. 114, 1791–1804.
Maritorena, S., Morel, A., Gentili, B., 1994. Diffuse reflectance of oceanic shallow waters: influence of water depth and bottom albedo. Limnol. Oceanogr. 39, 1689–1703.
Maritorena, S., Siegel, D.A., Peterson, A.R., 2002. Optimization of a semianalytical ocean color model for global-scale applications. Appl. Opt. 41, 2705–2714.
Markager, S., Vincent, W.F., 2000. Spectral light attenuation and the absorption of UV and blue light in natural waters. Limnol. Oceanogr. 45, 642–650.
Matsuoka, A., Hooker, S., Bricaud, A., Gentili, B., Babin, M., 2013. Estimating absorption coefficients of colored dissolved organic matter (CDOM) using a semi-analytical algorithm for southern Beaufort Sea waters: application to deriving concentrations of dissolved organic carbon from space. Biogeosciences 10, 917–927.
Matthews, M.W., 2011. A current review of empirical procedures of remote sensing in inland and near-coastal transitional waters. Int. J. Remote Sens. 32, 6855–6899.
Menon, H.B., Sangekar, N.P., Lotliker, A.A., Vethamony, P., 2011. Dynamics of chromophoric dissolved organic matter in Mandovi and Zuari estuaries – a study through in situ and satellite data. ISPRS J. Photogramm. Remote Sens. 66, 545–552.
Mobley, C.D., 1999. Estimation of the remote-sensing reflectance from above-surface measurements. Appl. Opt. 38, 7442–7455.
Morel, A., 1974. Optical properties of pure water and pure sea water. Opt. Aspects Oceanogr. 1, 1–24.
Odermatt, D., Gitelson, A., Brando, V.E., Schaepman, M., 2012. Review of constituent retrieval in optically deep and complex waters from satellite imagery. Remote Sens. Environ. 118, 116–126.
Olmanson, L.G., Brezonik, P.L., Finlay, J.C., Bauer, M.E., 2016. Comparison of Landsat 8 and Landsat 7 for regional measurements of CDOM and water clarity in lakes. Remote Sens. Environ.
Palmer, S.C., Kutser, T., Hunter, P.D., 2015. Remote sensing of inland waters: challenges, progress and future directions. Remote Sens. Environ. 157, 1–8.
Pope, R.M., Fry, E.S., 1997. Absorption spectrum (380–700 nm) of pure water. II. Integrating cavity measurements. Appl. Opt. 36, 8710–8723.
Powell, M.J., 1968. A FORTRAN Subroutine for Solving Systems of Nonlinear Algebraic Equations. Atomic Energy Research Establishment, Harwell (England).
Raymond, P.A., Oh, N.H., 2007. An empirical study of climatic controls on riverine C export from three major US watersheds. Global Biogeochem. Cycles 21.
Shanmugam, P., 2011. New models for retrieving and partitioning the colored dissolved organic matter in the global ocean: implications for remote sensing. Remote Sens. Environ. 115, 1501–1521.
Siegel, D., Maritorena, S., Nelson, N., Hansell, D., Lorenzi-Kayser, M., 2002. Global distribution and dynamics of colored dissolved and detrital organic materials. J. Geophys. Res.: Oceans (1978–2012) 107. 21-21-21-14.
Spedding, T., Hamel, C., Mehuys, G., Madramootoo, C., 2004. Soil microbial dynamics in maize-growing soil under different tillage and residue management systems. Soil Biol. Biochem. 36, 499–512.
Stedmon, C., Markager, S., Kaas, H., 2000. Optical properties and signatures of chromophoric dissolved organic matter (CDOM) in Danish coastal waters. Estuar. Coast. Shelf Sci. 51, 267–278.
Tian, Y.Q., Yu, Q., Feig, A.D., Ye, C., Blunden, A., 2013. Effects of climate and land-surface processes on terrestrial dissolved organic carbon export to major US coastal rivers. Ecol. Eng. 54, 192–201.
Tranvik, L., 2014. Carbon cycling in the Arctic. Science 345, 870.
Vodacek, A., Blough, N.V., DeGrandpre, M.D., Peltzer, E.T., Nelson, R.K., 1997. Seasonal variation of CDOM and DOC in the Middle Atlantic Bight: terrestrial inputs and photooxidation. Limnol. Oceanogr. 42, 674–686.
Volpe, V., Silvestri, S., Marani, M., 2011. Remote sensing retrieval of suspended sediment concentration in shallow waters. Remote Sens. Environ. 115, 44–54.
Watanabe, F., Mishra, D.R., Astuti, I., Rodrigues, T., Alcântara, E., Imai, N.N., Barbosa, C., 2016. Parametrization and calibration of a quasi-analytical algorithm for tropical eutrophic waters. ISPRS J. Photogram. Remote Sens. 121, 28–47.
Yang, W., Matsushita, B., Chen, J., Fukushima, T., 2011. A relaxed matrix inversion method for retrieving water constituent concentrations in case II waters: the case of Lake Kasumigaura, Japan. Geosci. Remote Sens., IEEE Trans. 49, 3381–3392.
Yang, W., Matsushita, B., Chen, J., Yoshimura, K., Fukushima, T., 2013. Retrieval of inherent optical properties for turbid inland waters from remote-sensing reflectance. IEEE Trans. Geosci. Remote Sens. 51, 3761–3773.
Zhao, J., Barnes, B., Melo, N., English, D., Lapointe, B., Muller-Karger, F., Schaeffer, B., Hu, C., 2013. Assessment of satellite-derived diffuse attenuation coefficients and euphotic depths in south Florida coastal waters. Remote Sens. Environ. 131, 38–50.
Zhu, W., Tian, Y.Q., Yu, Q., Becker, B.L., 2013a. Using Hyperion imagery to monitor the spatial and temporal distribution of colored dissolved organic matter in estuarine and coastal regions. Remote Sens. Environ. 134, 342–354.
Zhu, W., Yu, Q., 2013. Inversion of chromophoric dissolved organic matter from EO-1 hyperion imagery for turbid estuarine and coastal waters. Geosci. Remote Sens., IEEE Trans. 51, 3286–3298.
Zhu, W., Yu, Q., Tian, Y., Becker, B., Carrick, H., 2015. Issues and potential improvement of multiband models for remotely estimating Chlorophyll-a in complex inland waters. IEEE J. Selected Top. Appl. Earth Observ. Remote Sens.
Zhu, W., Yu, Q., Tian, Y.Q., 2013b. Uncertainty analysis of remote sensing of colored dissolved organic matter: evaluations and comparisons for three rivers in North America. ISPRS J. Photogram. Remote Sens. 84, 12–22.
Zhu, W., Yu, Q., Tian, Y.Q., Becker, B.L., Zheng, T., Carrick, H.J., 2014. An assessment of remote sensing algorithms for colored dissolved organic matter in complex freshwater environments. Remote Sens. Environ. 140, 766–778.